Optimizing Stellarators for Turbulent Transport

H. E. Mynick,[1] N. Pomphrey,[1] and P. Xanthopoulos[2]

[1]*Plasma Physics Laboratory, Princeton University, Princeton, New Jersey 08543, USA*

[2]*Max-Planck-Institut für Plasmaphysik, Teilinstitut Greifswald, 17491 Greifswald, Germany*

(Received 11 May 2010; published 27 August 2010)

Up to now, the term ''transport-optimized'' stellarators has meant optimized to minimize neoclassical transport, while the task of also mitigating turbulent transport, usually the dominant transport channel in such designs, has not been addressed, due to the complexity of plasma turbulence in stellarators. Here, we demonstrate that stellarators can also be designed to mitigate their turbulent transport, by making use of two powerful numerical tools not available until recently, namely, gyrokinetic codes valid for 3D nonlinear simulations and stellarator optimization codes. Two initial proof-of-principle configurations are obtained, reducing the level of ion temperature gradient turbulent transport from the National Compact Stellarator Experiment baseline design by a factor of 2–2.5.

DOI: 10.1103/PhysRevLett.105.095004 PACS numbers: 52.55.Hc, 52.35.Ra, 52.65.Tt

Transport due to plasma turbulence has been a major challenge for magnetic confinement since the inception of the fusion program in the 1950s. Starting in the 1980s, a number of approaches to neoclassical-transport-optimized stellarators were discovered [1–5], in which the high neoclassical (NC) transport levels attributed to classical stellarators could be substantially reduced, to a level making stellarator confinement comparable to that achievable in tokamaks, dominated by turbulent or ''anomalous'' transport. In recent years, two powerful numerical tools have been developed, which also make mitigating turbulent transport in stellarators a realistic possibility, namely, configuration optimization codes such as STELLOPT [6], and gyrokinetic (GK) codes valid for 3D configurations, such as the GENE/GIST code package [7,8]. In this Letter, we make use of these two new tools to demonstrate that new stellarator configurations with appreciably diminished turbulent transport levels can be evolved from stellarators designed without this turbulent-transport optimization, raising the prospect of a new class of stellarators with greatly improved overall confinement.

STELLOPT seeks to minimize a cost function $C^2(\mathbf{z}) = \sum_i w_i^2 C_i^2(\mathbf{z})$ in the ''shape space'' $\mathbf{z} \equiv \{z_j\}$ specifying a stellarator design, where the C_i^2 are the contributions from any physics or engineering criteria the user wishes to apply, and the w_i are adjustable weights. (For the fixed-boundary equilibria we compute here, the z_j are the Fourier amplitudes specifying the boundary shape of the design. One could equally well take free-boundary equilibria, with the z_j the currents in the coil set.) For the turbulent contribution C_t^2, one could ideally take $C_t = \langle Q_{\rm GK} \rangle$, the surface- or volume-averaged heat flux $Q_{\rm GK}$ from nonlinear GENE runs, but this would be far too computationally expensive, since many hundreds of individual configurations are evaluated in a typical optimizer run, and a nonlinear GK parallel simulation for a single flux tube for the present application requires on the order of 100 CPU days. To surmount this obstacle, we instead employ a ''proxy function'' $Q_{\rm prox}$ in C_t^2 to stand in place of $Q_{\rm GK}$, a fairly simple function of key input geometric quantities, based on theory and on the geometry dependences of $Q_{\rm GK}$ found in GENE studies on a family of NC-optimized stellarators [9]. $Q_{\rm prox}$ need not give a highly accurate prediction of what the GK result will be (though of course the more accurate the better)—it need only capture enough of the physics to guide the optimizer toward configurations which GENE will subsequently confirm has reduced $Q_{\rm GK}$. Moreover, by examining the means by which STELLOPT contrives to improve $Q_{\rm prox}$ and $Q_{\rm GK}$, one may learn methods for deforming the stellarator shape to achieve the turbulent stabilization which are geometrically possible, whose discovery without the optimizer would be extremely difficult.

For $Q_{\rm prox}$, we begin with an expression for the ion radial heat flux $Q_i = -\chi n_0 g^{xx} dT_i/dx$, with radial coordinate $x \equiv (2\psi_t/B_a)^{1/2}$, $2\pi\psi_t$ the toroidal flux, B_a the magnetic field strength B at the plasma edge (where $x = a$), and $g^{xx} \equiv |\nabla x|^2$ the xx component of the metric tensor. We use the quasilinear expression for the ion conductivity, $\chi = \sum_{\mathbf{k}} D_{\mathbf{k}}$, with

$$D_{\mathbf{k}} = (\omega_{*i} L_n)^2 \left\langle \left| \frac{e\phi_{\mathbf{k}}}{T_i} \right|^2 \right\rangle \gamma_{\mathbf{k}}/\omega_{\mathbf{k}}^2 \simeq c_D \gamma_{\mathbf{k}}/k_x^2. \quad (1)$$

Here, $\omega_{*i} \equiv -(ck_y T_i/eB)\kappa_n$ is the diamagnetic frequency, with inverse density scale length $\kappa_n \equiv L_n^{-1} \equiv -\partial_x \ln n_0$ and $k_y \equiv \mathbf{k} \cdot \hat{y}$ the wave vector component in the binormal direction $\hat{y} \equiv \hat{b} \times \hat{x}$, with $\hat{x}$ and $\hat{b}$ unit vectors in the directions normal to a flux surface and along the magnetic field. The final form is obtained using a simple mixing-length argument for the mean-square potential fluctuation amplitude $\langle |\phi_{\mathbf{k}}|^2 \rangle$, with c_D a multiplicative constant, determined below.

As in Ref. [9], for simplicity we consider only ion temperature gradient (ITG) turbulence [10] with adiabatic

electrons. As found there, two geometric quantities central to determining the form and amplitude of the turbulence are the "radial curvature" $\kappa_1 \equiv \mathbf{e}_x \cdot \boldsymbol{\kappa}$, with vector curvature $\boldsymbol{\kappa}$ and $\mathbf{e}_x$ the covariant basis vector for x [8], and the local shear $s_l \equiv \partial_\theta (g^{xy}/g^{xx})$, with θ the poloidal azimuth in flux coordinates, which parametrizes distance along a field line. An approximate ITG dispersion equation is

$$0 \simeq \frac{1}{\tau} + \frac{\omega_{*i}(1+\eta_i)\omega_{di}}{\omega^2} + \frac{k_\parallel^2 v_i^2 \omega_{*i}(1+\eta_i)}{\omega^3}, \quad (2)$$

with $\omega_{di} = -\omega_{*i}\kappa_1/\kappa_n$ the ion drift frequency, $\eta_i \equiv \kappa_T/\kappa_n$, and $\kappa_T \equiv -\partial_x \ln T_i$. The first term on the right side is the adiabatic electron contribution, the second term gives the ITG "toroidal branch", and the third term gives the "slab branch". If that 3rd term is neglected, Eq. (2) is quadratic in ω, giving $\omega \equiv \pm i\gamma_\mathbf{k} \simeq \pm\omega_{*i}[\tau(1+\eta_i)\kappa_1/\kappa_n]^{1/2}$, becoming unstable for $\kappa_1 < 0$ ("bad curvature"). This expression has a critical pressure gradient $\kappa_{cr} = 0$, which becomes nonzero for a more complete dispersion equation, e.g., from including the 3rd term in Eq. (2). Here, we include κ_{cr} simply as a parameter, by making the replacement $(1+\eta_i) \equiv \kappa_p/\kappa_n \rightarrow (\kappa_p - \kappa_{cr})/\kappa_n$. Then one has

$$\gamma_\mathbf{k} \simeq (\omega_{*i}/\kappa_n)|\tau\kappa_1(\kappa_p - \kappa_{cr})|^{1/2} H(\kappa_p - \kappa_{cr}) H(-\kappa_1), \quad (3)$$

with $H(\kappa)$ the Heaviside function. Retaining the 3rd term in Eq. (2), and making the replacement $k_\parallel \rightarrow -(i/qR)\partial_\theta$ (with R the major radius and q the safety factor), yields a Schrödinger equation, which localizes the mode in θ to wells in the effective potential $V_{eff}(\theta)$, proportional to the first two terms in Eq. (2) [9].

We model k_x^{-2} on the intuition that s_l plays a role similar to that played by flow shear [9], stabilizing the mode and diminishing its radial extent from the "mesoscale" ($k_x^{-1} \sim \sqrt{L_p \rho_i}$) to a microscale ($k_x^{-1} \sim \rho_i$) when the $E \times B$ shearing frequency ω_E becomes comparable to the inverse correlation time τ_E^{-1} for fluctuations in the absence of $E \times B$ flow [11]:

$$k_x^{-2}(\omega_E, s_l) \simeq \rho_i^2 + \rho_i L_p/[1 + (\tau_E\omega_E)^2 + \langle(\tau_s s_l)^2\rangle_{\Delta\theta}]. \quad (4)$$

Here, ρ_i is the ion gyroradius, $L_p \equiv \kappa_p^{-1}$, τ_E, τ_s are constants set below, and $\langle\cdot\rangle_{\Delta\theta}$ is an average along a field line weighted by a Gaussian of width $\Delta\theta$, a simple means of giving k_x^{-2} the nonlocal character more rigorously imposed by actually solving the mode equation noted above along $\mathbf{B}$. Q_{prox} is thus determined by Eqs. (1), (3), and (4), which have 5 as yet undetermined constants, κ_{cr}, τ_E, τ_s, $\Delta\theta$, and c_D. Here, we neglect the flow-shear contribution (we set $\tau_E = 0$) and fix the remaining 4 by using simulated annealing [12] to make a best fit of Q_{prox} with the Q_{GK} from the results of GENE simulations on the family of 3 flux tubes in each of 4 toroidal configurations studied in Ref. [9], giving values 0.053, 1.12, 0.207, and 0.959, respectively. A comparison of Q_{prox} (solid lines) and Q_{GK} (dashed lines) along one field line of each of these 4 configurations is given in Fig. 1. For all flux tubes simulated, Q_{prox} represents reasonably well the form of Q_{GK} along $\mathbf{B}$, and also gives the approximate magnitude in each case but for 2 of the 3 tubes simulated for W7X (Wendelstein VII-X) [13], where it is too small by a factor of about 3, indicating that some further physics is to be found to improve the present Q_{prox}. The predictive reliability of C_t^2 is somewhat better than that indicated in Fig. 1, since it uses the surface average $\langle Q_{prox}\rangle$ of Q_{prox}, and the local disparities in $(Q_{prox} - Q_{GK})$ tend to cancel.

In Fig. 2–4 we show the results of two STELLOPT runs using this Q_{prox}. The Levenberg-Marquardt optimization

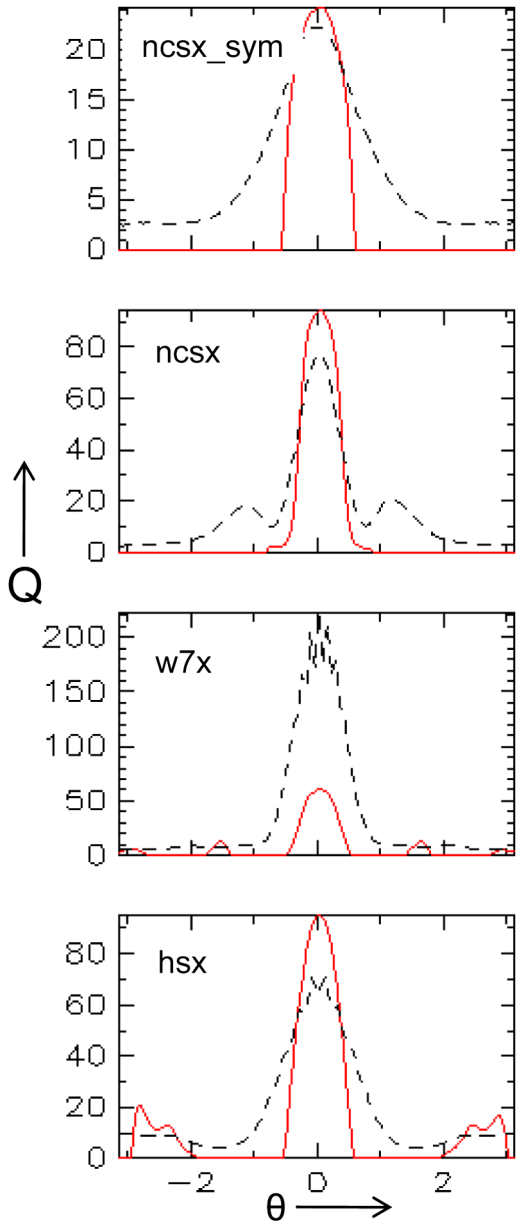

FIG. 1 (color online). Comparison of Q_{prox} (red solid line) with Q_{GK} (black dashed line) for one flux tube of each of the 4 toroidal configurations studied in Ref. [9].

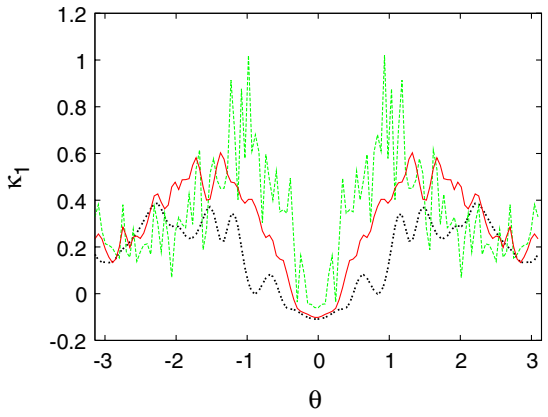

FIG. 2 (color online). Comparison of radial curvature $\kappa_1(\theta)$ for 1 poloidal transit for NCSX (heavy dashed black line), QA_35q [dashed gray) green line], and QA_40n (solid red line).

scheme [14] STELLOPT uses runs in successive "generations" of equilibria, here each with 54 members (one for each direction of shape space $\mathbf{z}$), to determine the direction in $\mathbf{z}$ space to move next. For both cases, STELLOPT begins with configuration LI383, which formed the baseline configuration for National Compact Stellarator Experiment (NCSX) [15], at $\beta = 4.2\%$. w_t is made large enough to make C_t^2 dominate C^2 for the first several generations. Constraints are also applied to maintain the plasma β, aspect ratio, and RB_t (= major radius × toroidal field), but the configurations are otherwise unconstrained. After several generations, a sample equilibrium is chosen from each run, before the configurations become less interesting from a practical standpoint (for example, their rotational transform dropping excessively). We select a sample configuration "QA_35q" from generation 4 of the first run, and "QA_40n" from generation 7 of the second. C_t is 2 orders of magnitude below that of NCSX for QA_35q, and about 1 order of magnitude for QA_40n. The reason why is shown in Fig. 2, which compares radial curvature $\kappa_1(\theta)$ for 1 poloidal transit for NCSX (dashed black line) with those for QA_35q [dashed gray (green) line] and QA_40n (solid red). For both new configurations, one sees that STELLOPT has found a means of boosting κ_1 so that it has bad curvature ($\kappa_1 < 0$) in a much narrower region than NCSX and worse curvature than NCSX only where $\kappa_1 > 0$ for both configurations. While QA_40n has a κ_1 which is somewhat more oscillatory than for NCSX, and more so for QA_35q, both have smooth, converged VMEC [16] equilibria. In Fig. 3 we show the boundaries of NCSX (dashed black line) and QA_40n (solid red line) for cross sections at 4 values of toroidal azimuth ζ. The boundaries for QA_35q are similar to those of QA_40n.

While C_t has fallen orders of magnitude from that of NCSX, the decisive test of whether the new configurations truly have reduced transport is from nonlinear GENE runs. This comparison is given in Fig. 4, showing the line averaged Q_{GK} for NCSX (dashed black line), QA_35q [dashed gray (green) line] and QA_40n (solid red line) versus time. One sees that both indeed have Q_{GK} substantially diminished from that for NCSX, by a factor of about 2.5 for QA_35q and about 2 for QA_40n. The reduction is not as large as indicated by Q_{prox}, but the proxy is clearly adequate to guide STELLOPT in the direction needed to reduce the turbulent transport. The achieved reduction is quite appreciable, comparable to the reduction achieved in tokamaks in going from L to H mode.

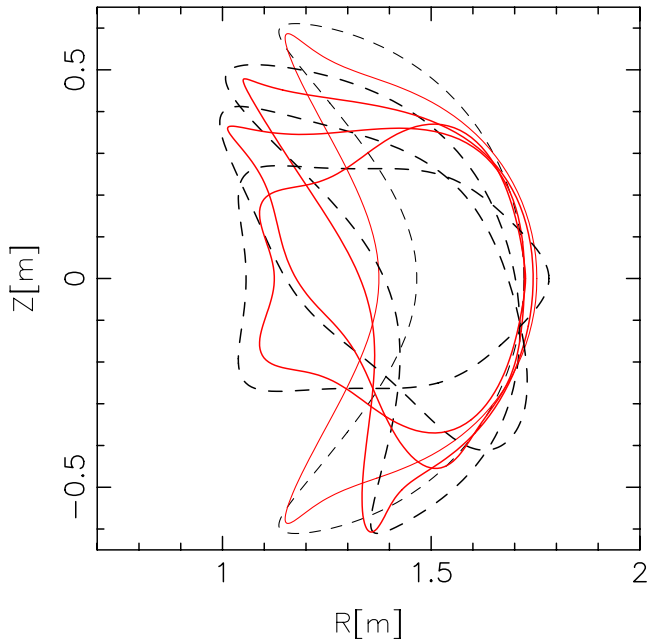

FIG. 3 (color online). Comparison of boundary shapes of NCSX (dashed black line) and QA_40n (solid red line) at values of $N\zeta$ (= number of field periods × toroidal angle) = $0, \pm\pi/2, \pi$.

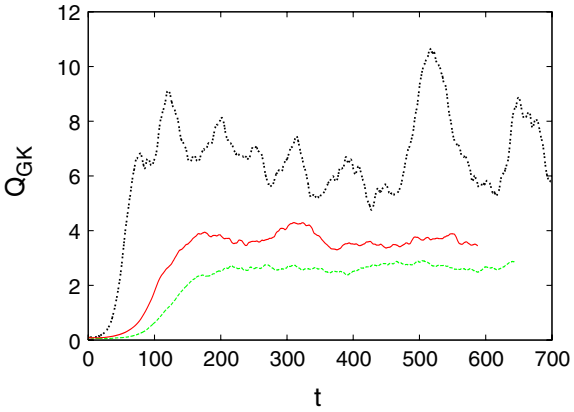

FIG. 4 (color online). Comparison of line-averaged heat flux Q_{GK} versus time for NCSX (heavy dashed black line), QA_35q [dashed gray (green) line], and QA_40n (solid red line) from nonlinear GENE runs. QA_35q and QA_40n achieve reductions in turbulent transport over that in NCSX by factors of about 2.5 and 2, respectively.

While QA_35q fares somewhat better than QA_40n in its Q_{prox} and Q_{GK}, it does worse in its NC transport level, as assessed by its "$1/\nu$" NC value $Q_{\mathrm{NC}} \sim \epsilon_{\mathrm{eff}}^{3/2}/\nu$, with ϵ_{eff} the configuration's "effective ripple strength," and ν the thermal collision frequency. QA_35q has $\epsilon_{\mathrm{eff}}^{3/2}$ about 30 times that of NCSX. However, the high degree of NC optimization present in NCSX makes its predicted ripple transport smaller than that of its estimated turbulent transport by about the same amount [17], so that NC transport is still not dominant for this configuration. In contrast, QA_40n actually has *better* Q_{NC} than NCSX, with $\epsilon_{\mathrm{eff}}^{3/2}$ about 0.6 times that of NCSX.

QA_35q and QA_40n were arrived at using almost the same STELLOPT parameters, the main difference being the selection of different representations for the boundary in producing the equilibria. This small difference set STELLOPT on two similar but different courses through shape space, owing largely to the highly structured topography of $C^2(\mathbf{z})$. These two systems provide the first "proof of principle" that substantial turbulence mitigation can indeed be achieved by 3D shaping using this approach. However, in evolving them, STELLOPT did not apply various constraints to the configurations to make them fully satisfactory. For example, while mostly ballooning stable, as is LI383, QA_35q and QA_40n are kink unstable, and their rotational transforms are smaller than that of LI383 by factors of about 2.7 and 1.6, respectively. As found from earlier experience in finding attractive candidate designs, including, for example, LI383 and the N3ARE design derived from it [18,19], finding configurations satisfying multiple constraints can often be achieved, but the trajectory through shape space is a multistaged process, requiring human assessment and adjustment.

Many further possibilities exist for making use of this general approach to turbulent transport mitigation. The reduction STELLOPT achieved in QA_35q and QA_40n principally made use of the κ_1 dependence of Q_{prox}, finding a means of deforming NCSX to restrict the domain of bad curvature, and thereby alleviate the ITG instability. In a similar way, one may seek other configurations which reduce transport by using the s_l dependence in Q_{prox}. Also, as noted, the present Q_{prox} can be improved as a model for ITG transport, and one may expect further improvements would accrue as more of the significant physics in Q_{GK} is captured by Q_{prox}. Further, the present restriction to ITG turbulence was taken only for simplicity—any modes which GK codes such as GENE can compute (e.g., trapped-electron or electron temperature-gradient modes) can be addressed by this method, developing a modified Q_{prox} guided by theory and by GK studies of Q_{GK}. Moreover, it will also be of interest to use starting designs other than NCSX, to see what different means of achieving transport reduction STELLOPT finds as the initial configuration is varied. For example, each of the NC-transport-optimized designs studied in Ref. [9], and perhaps tokamaks, would provide an edifying test bed for this approach. Work addressing these avenues has been initiated.

The authors are grateful to A. Boozer, L. Maingi, G. Rewoldt, and E. Valeo for valuable discussions. This work supported by U.S. Department of Energy Contract No. DE-AC02-09CH11466. Some of the GENE simulations were performed at the Jülich Supercomputing Center (JSC).

[1] H. E. Mynick, T. K. Chu, and A. H. Boozer, Phys. Rev. Lett. **48**, 322 (1982).
[2] A. H. Boozer, Phys. Fluids **26**, 496 (1983).
[3] J. Nührenberg and R. Zille, Phys. Lett. A **129**, 113 (1988).
[4] J. Nührenberg, W. Lotz, and S. Gori, in *Theory of Fusion Plasmas*, edited by E. Sindoni, F. Tryon, and J. Vaclavik (Societá Italiana di Fisica, Bologna, 1994).
[5] P. R. Garabedian, Phys. Plasmas **3**, 2483 (1996).
[6] A. Reiman *et al.*, Plasma Phys. Controlled Fusion **41**, B273 (1999).
[7] F. Jenko, W. Dorland, M. Kotschenreuther, and B. N. Rogers, Phys. Plasmas **7**, 1904 (2000).
[8] P. Xanthopoulos, W. A. Cooper, F. Jenko, Yu. Turkin, A. Runov, and J. Geiger, Phys. Plasmas **16**, 082303 (2009).
[9] H. E. Mynick, P. Xanthopoulos, and A. H. Boozer, Phys. Plasmas **16**, 110702 (2009).
[10] F. Romanelli, Phys. Fluids B **1**, 1018 (1989).
[11] J. Garci'a, K. Yamazaki, J. Dies, and J. Izquierdo, Plasma Phys. Controlled Fusion **48**, 15 (2006).
[12] Wm. H. Press *et al.*, *Numerical Recipes in FORTRAN 77* (Cambridge University Press, Cambridge, England, 1996), pp. 436ff.
[13] G. Grieger, W. Lotz, and P. Merkel *et al.*, Phys. Fluids B **4**, 2081 (1992).
[14] Wm. H. Press *et al.*, *Numerical Recipes in FORTRAN 77* (Ref. [12]), pp. 676ff.
[15] G. H. Neilson, M. C. Zarnstorff, J. F. Lyon, and the NCSX Team, J. Plasma Fusion Res. **78**, 214 (2002).
[16] S. P. Hirshman, W. I. van Rij, P. Merkel, Comput. Phys. Commun. **43**, 143 (1986).
[17] D. R. Mikkelsen, H. Maassberg, M. C. Zarnstorff, C. D. Beidler, W. A. Houlberg, W. Kernbichler, H. Mynick, D. A. Spong, P. Strand, and V. Tribaldos, Fusion Sci. Technol. **51**, 166 (2007).
[18] L. P. Ku and P. Garabedian, Fusion Sci. Technol. **50**, 207 (2006).
[19] H. E. Mynick, A. H. Boozer, and L.-P. Ku, Phys. Plasmas **13**, 064505 (2006).